



Tuning the Interfacial and Energetic Interactions between a Photoexcited Conjugated Polymer and Open-Shell Small Molecules

Journal:	<i>Soft Matter</i>
Manuscript ID	SM-ART-09-2018-001930.R1
Article Type:	Paper
Date Submitted by the Author:	10-Dec-2018
Complete List of Authors:	Wilcox, Daniel; Purdue University, Davidson School of Chemical Engineering Snaider, Jordan; Purdue University, Chemistry Mukherjee, Sanjoy; University of California Santa Barbara, Yuan, Long; Purdue University, Chemistry Huang, Libai; Purdue University, Department of Chemistry Savoie, Brett; Purdue University School of Chemical Engineering Boudouris, Bryan; Purdue University, Davidson School of Chemical Engineering



Journal Name

ARTICLE

Tuning the Interfacial and Energetic Interactions between a Photoexcited Conjugated Polymer and Open-Shell Small Molecules

Received 00th January 20xx,
Accepted 00th January 20xx

DOI: 10.1039/x0xx00000x

www.rsc.org/

Daniel A. Wilcox,^a Jordan Snaider,^b Sanjoy Mukherjee,^{a,c} Long Yuan,^b Libai Huang,^b Brett M. Savoie,^a and Bryan W. Boudouris^{a,b,*}

Design rules and application spaces for closed-shell conjugated polymers have been well established in the field of organic electronics, but the emerging class of open-shell stable radicals have not been evaluated in such detail. Thus, establishing the underlying physical phenomena associated with the interactions between both classes of molecules is imperative for the effective utilization of these soft materials. Here, we establish that Förster Resonance Energy Transfer (FRET) is the dominant mechanism by which energy transfer occurs from a common conjugated polymer to various radical species using a combination of experimental and computational approaches. Specifically, we determined this fact by monitoring the fluorescence quenching of poly(3-hexylthiophene) (P3HT) in the presence of three radical species: (1) the galvinoxyl; (2) the 2-phenyl-4,4,5,5-tetramethylimidazoline-3-oxide-1-oxyl (PTIO); and (3) the 4-hydroxy-2,2,6,6-tetramethylpiperidine-1-oxyl (TEMPO) radicals. Both in solution and in the solid-state, the galvinoxyl and PTIO radicals showed quenching that was on par with that of a common fullerene electron-accepting derivative, due to the considerable overlap of their absorbance spectrum with the fluorescence spectrum of the P3HT species, which indicated that isoenergetic electronic transitions existed for both species. Conversely, TEMPO showed minimal quenching at similar concentrations due to the lack of such an overlap. Furthermore, computational studies demonstrated that FRET would occur at a significantly faster rate than other competing processes. These findings suggest that long-range energy transfer can be accomplished in applications when radicals that can act as FRET acceptors are utilized, forming a new design paradigm for future applications involving both closed- and open-shell soft materials.

Introduction

The self-assembly and interfacial interactions of soft materials in the active layers of organic electronic devices are offering new perspectives on the modern energy conversion and energy storage landscape.¹ For example, the commercialization of organic light-emitting devices (OLEDs)² and the potential associated with the low-cost production of other electronic devices (e.g., batteries, sensors, thermoelectric modules, and photovoltaic cells) has resulted in significant interest in these materials from academic, military, and commercial entities.³ To date, most organic electronic devices utilize molecules and molecular blends with extensive π -conjugation, which allows for the stabilization of ionized states

on the molecule, subsequently permitting the conduction of charge.^{3,4} Due to the significant research investments in this initial wave of organic electronics research, molecular design rules and defined structure-property relationships for closed-shell conjugated polymers as well as the structural, energetic, and electronic interactions between different conjugated species are relatively well understood. However, this same methodology has not been extended to radical-containing organic electronic systems. This is despite the promise that many of these materials show with respect to charge, energy, and spin transfer (e.g., spin-manipulating) platforms that are not always well-addressed by closed-shell conjugated polymers.^{5,6} Thus, there is a critical need to establish the key interactions of stable organic radicals with macromolecules and their role as charge and energy transfer moieties in organic electronic systems.

Stable organic radicals, which contain one or more unpaired electrons in their molecular structure, can undergo oxidation or reduction to form stable ionic species. Therefore, charge can be transferred to (or from) individual radical sites and transported within specific domains of these materials through electron self-exchange reactions in the solid state. As with conjugated materials, radicals are classified based upon whether they are preferentially oxidized (p-type) or reduced (n-type). Materials

^a Charles D. Davidson School of Chemical Engineering, Purdue University, 480 W Stadium Ave, West Lafayette, Indiana 47907, United States.

^b Department of Chemistry, Purdue University, 560 Oval Drive, West Lafayette, Indiana 47907, United States

^c Present Address: Mitsubishi Chemicals Center for Advanced Materials, 3107 Materials Research Laboratory, University of California Santa Barbara, Santa Barbara, CA 93106-5150.

Electronic Supplementary Information (ESI) available: solution phase absorbance and fluorescence spectra of the P3HT-Quencher solutions, absorbance spectra of the galvinoxyl and PTIO anions, AFM images, and details about the inner-filter effect correction. See DOI: 10.1039/x0xx00000x

capable of readily undergoing both types of redox reactions (i.e., to form either a cationic or anionic species) are referred to as ambipolar. Radical materials are also frequently referred to as “open-shell” materials, indicating that they have partially-filled frontier molecular orbitals, to distinguish them from traditional “closed-shell” materials where these orbitals are completely filled. In recent years, the potential value of these radical-based materials has been demonstrated through conducting polymer⁷ applications and with their utilization as active interfacial-modifying layers in organic and perovskite solar cells,^{8,9} organic field-effect transistors,¹⁰ and as dopants in thermoelectric applications.^{11–13} Additionally, the non-zero spin of the stable radical species makes them excellent candidates for applications where manipulation of the spin states within a given system are desired.¹⁴ While radical-based materials are now being used in conjunction with conjugated polymers, the fundamental interactions and energy transfer events in these closed-shell–open-shell hybrid composites have not been well illustrated in the literature. Indeed, recent results looking at radical moieties covalently linked to a conjugated polymer backbone illustrate the importance of tuning the energetic interactions between both functionalities to optimize the end behavior of the composite material, in this case, for organic radical battery applications.^{15–17} In order to more effectively establish the potential application space of this emerging class of materials, the interfacial and energetic interactions between conjugated materials and radical-based materials must be deciphered in full.

Specifically, the behavior of the excited states in conjugated polymer systems can be elucidated by evaluating the fluorescent behavior of the macromolecules. In a system of two different molecular species, the quenching of fluorescence is a direct reflection of the intermolecular interactions of the pair.¹⁸ Many conjugated polymer species are fluorescent, and recent studies have demonstrated that fluorescent radical species containing conjugated units exist, which are being actively researched for utilization in OLEDs as their emission from doublet excited states elegantly avoids the 75% loss in quantum efficiency caused by formation of triplet excited states in conventional closed-shell materials.^{19,20} Nevertheless, the vast majority of stable open-shell materials are non-fluorescent, owing to their open-shell electronic structure, which facilitates non-radiative decay of their excited states. Based on this concept, open-shell moieties such as the 2,2,6,6-tetramethylpiperidine-1-oxyl (TEMPO) radical have often been used as fluorescence quenchers for a variety of soft materials including both conjugated small molecules^{21–25} and quantum dots.^{26–28} In these studies, a variety of mechanisms, including electron transfer, resonance energy transfer, and enhanced intersystem crossing, have been proposed. Here, we establish the principal molecular interactions by which fluorescence quenching between a radical species and a specific conjugated polymer, poly(3-hexylthiophene) (P3HT) occurs, as P3HT has served as an oft-used material in many organic electronic applications.²⁹ Through a combination of experiment and simulation, we demonstrate that Förster Resonance Energy Transfer (FRET) is the primary mechanism by which the

fluorescence quenching occurs in P3HT for radical species that absorb light strongly within the visible range, and that radical species with low optical absorption coefficients do not show significant quenching behavior. Thus, certain interactions become improbable, which allows for the strategic design of systems that utilize both conjugated and radical species. This key point has significant implications in the development of coupled closed-shell conjugated polymer-radical molecule systems and interfaces with tunable directional energy transport.

Materials and Methods

Materials

The 4-hydroxy-2,2,6,6-tetramethylpiperidine-1-oxyl (TEMPO) radical (97%), galvinoxyl radical, L-ascorbic acid (99%), sodium hydride (95%), anhydrous chloroform (> 99%), and ethanol (200 proof) were purchased from Sigma-Aldrich. The 2-phenyl-4,4,5,5-tetramethylimidazoline-3-oxide-1-oxyl (PTIO) radical (> 98%) was purchased from TCI America, sodium hydroxide (> 98%) was purchased from Honeywell, poly(3-hexylthiophene) (P3HT) ($M_n \sim 60 \text{ kg mol}^{-1}$) was purchased from Rieke Metals, and phenyl-C₆₁-butyric acid methyl ester (PCBM) was purchased from Nano-C. All materials were used as received. Glass slides were purchased from Delta Technologies, and fused silica slides were purchased from Quartz Scientific, Inc.

Solution Phase Fluorescence Quenching

To generate the samples for the fluorescence quenching experiments, a solution of 0.01 mg of P3HT per 1 mL of chloroform was created (60 μM in terms of the number of thiophene repeat units). Quencher solutions composed of 3.4 mg mL⁻¹ TEMPO, 4.7 mg mL⁻¹ PTIO, 8.4 mg mL⁻¹ galvinoxyl, and 18.2 mg mL⁻¹ PCBM in chloroform were mixed in order to make each solution have a molar concentration of 20 mM. Using a transfer pipette, 3 mL of the P3HT solution were added to a cuvette for fluorescence measurements. A cap was placed over the cuvette to minimize solvent evaporation. The fluorescence spectrum of the solution was measured using a Cary Eclipse Fluorescence Spectrophotometer over a wavelength range of 525 nm $\leq \lambda \leq$ 900 nm with an excitation wavelength of 500 nm. Afterwards, 15 μL of a specific quencher solution were added to the P3HT solution using a transfer pipette. This resulted in a quencher concentration of 0.1 mM. The pipette was pumped multiple times to ensure mixing, then the cuvette was capped. The fluorescence spectrum was obtained, and the procedure was repeated, increasing the quencher concentration in 0.1 mM increments up to a concentration of 1.0 mM.

After acquiring the fluorescence spectra, the ultraviolet-visible (UV-Vis) absorbance spectra were acquired, using a Cary 60 Spectrometer over a wavelength range of 250 nm $\leq \lambda \leq$ 1,100 nm with chloroform serving as a blank. This was done within three hours of taking the fluorescence spectra, using the same P3HT and quencher solutions that were prepared previously. To minimize degradation, as P3HT and the galvinoxyl radical (in solution) are air-sensitive, the solutions were divided in half

after preparation. One half was used for the fluorescence measurements and the other half was kept under nitrogen atmosphere in a glovebox until the absorbance measurements were performed. The P3HT and quencher solutions were mixed using the same procedure as for the fluorescence measurements: 15 μL of quencher solution were added to the P3HT solution, increasing the concentration to 0.1 mM, and the absorbance spectra were taken. This was repeated up to a quencher concentration of 1.0 mM.

As the galvinoxyl and PTIO radicals and PCBM all have a high absorbance at the excitation and emission wavelengths, a significant decrease in the fluorescence signal occurred due to attenuation of the excitation beam and the emitted light. This apparent quenching, which is more accurately described as the inner-filter effect, was not caused by any actual interaction of the chemical species, and the raw data were corrected to account for this phenomenon. For a fluorimeter where the entire width of the sample is excited and the entire length is collected by the detector, as with the particular instrument used in the experiment,³⁰ the appropriate formula (see the Electronic Supplemental Information for the derivation of this equation) is as follows.

$$I_{corr} = \frac{\ln(10)^2 A_{Ex} A_{Em}}{(1 - 10^{-A_{Ex}})(1 - 10^{-A_{Em}})} I_{obs} \quad (1)$$

Here, I_{corr} is the corrected intensity, I_{obs} is the measured (observed) intensity, and A_{ex} and A_{em} are the absorbance values of the solution over the entire cuvette length at the excitation and emission wavelengths, respectively.³¹

Quencher Anion Absorbance Measurements

To measure the absorbance spectrum of the galvinoxyl anion, a 4 mM (1.68 mg mL⁻¹) solution of galvinoxyl in ethanol was prepared, along with a 40 mM (7.0 mg mL⁻¹) solution of ascorbic acid and a 100 mM (2.4 mg mL⁻¹) solution of sodium hydride, both in ethanol. The galvinoxyl and ascorbic acid solutions were mixed in equal proportions to yield a quenched galvinoxyl solution, and this solution was mixed with a proportional amount of sodium hydride solution to yield a solution containing 1 mM of the galvinoxyl anion. Another solution consisting of 1 part ethanol, 1 part ascorbic acid solution, and 2 parts sodium hydride solution was also prepared to use as a baseline for absorbance measurements. After mixing, both solutions were diluted to 1/100th of their original concentration. The UV-Vis absorbance spectrum of the dilute galvinoxyl solution was acquired, using a Cary 60 Spectrometer over a wavelength range of 300 nm $\leq \lambda \leq$ 1,100 nm with the dilute ascorbic acid/sodium hydride solution serving as a blank.

To measure the absorbance spectrum of the PTIO anion, a 4 mM (0.93 mg mL⁻¹) solution of PTIO in water was prepared, along with a 40 mM (7.0 mg mL⁻¹) solution of ascorbic acid and a 100 mM (4.0 mg mL⁻¹) solution of sodium hydroxide, both in water. As above, the PTIO solution was mixed with the ascorbic acid and sodium hydroxide solutions to yield a solution containing 1 mM of the PTIO anion. A baseline solution consisting of ascorbic acid and sodium hydroxide without the PTIO radical was also prepared. After mixing, both solutions

were diluted to 1/10th of their original concentration. This dilution is different than what was used for the galvinoxyl anion, due to the weaker absorbance of the PTIO anion. The UV-Vis absorbance spectrum of the dilute PTIO solution was acquired in the same manner using the dilute ascorbic acid-sodium hydroxide solution as a blank.

Thin Film Preparation

All solutions were prepared with a P3HT concentration of 10 mg mL⁻¹ in chloroform (60 mM repeat units). Stock solutions of 6.7 mM of each small molecule quencher were prepared in chloroform. For each solution, the appropriate amounts of chloroform and stock solution were added to the P3HT powder to provide for molar loadings of quencher between 0 and 10% (on a molar basis) in 2% increments. After preparation of the solutions in a nitrogen atmosphere, the solutions were allowed to stir for at least 3 h. Depending on the experiment, either 13.6 mm \times 15.6 mm borosilicate glass or 1-inch square fused silica substrates were cleaned by sonication for 10 minutes each in acetone, chloroform, and isopropyl alcohol, in a sequential manner. Afterwards, the appropriate solution was spun-coat on to the substrates at 1,500 rpm for 60 s in a nitrogen-filled glove box.

Thin Film Fluorescence Quenching

Thin films were cast onto fused silica slides using the above procedure. Once cast, the absorbance spectra of the films were measured using a Cary 60 Spectrometer over a wavelength range of 190 nm $\leq \lambda \leq$ 1,100 nm with a clean fused silica slide as a blank. Within an hour of taking the absorbance spectra, the fluorescence spectra were acquired using an Edinburgh Instruments FLS980 steady-state fluorescence spectrometer over a wavelength range of 550 nm $\leq \lambda \leq$ 800 nm with an excitation wavelength of 500 nm. A 550 nm colored glass long-pass filter purchased from ThorLabs Inc. was used as an emission filter.

Ensemble Transient Absorption Spectroscopy Measurements

Thin films were prepared on borosilicate glass substrates following the above procedure, except the concentrations of solids were doubled to yield thicker films with higher optical density values. The films were also encapsulated to prevent degradation during the measurements. This was achieved by placing the samples film side down on glass coverslips and sealing with a clear epoxy (JBWeld Clear Weld). Transient absorption spectra of the films were measured by a femtosecond pump-probe system with a home-built transient absorption spectrometer. Laser pulses at 1,030 nm with 250 fs duration were generated by a 400 kHz amplified Yb:KGW laser system (PHAROS, Light Conversion Ltd.). The probe beam was a white light continuum beam spanning the 450 nm $\leq \lambda \leq$ 950 nm spectral region, created by focusing 5% of the 1,030 nm fundamental output onto an yttrium aluminum garnet (YAG) crystal (4.0 mm thick). The rest of the output pumps an optical parametric amplifier (OPA, TOPAS-Twins, Light Conversion Ltd.) to generate pump pulses with tunable photon energies for the transient absorption experiments.

Atomic Force Microscopy (AFM) Imaging

Thin films were prepared on borosilicate glass substrates following the same procedure that was used for the steady-state thin film absorption measurements. AFM images were acquired using a Veeco Dimension 3100 AFM operating in tapping mode with MikroMasch HQ:NSC15/AI BS tips.

X-ray Diffraction

Borosilicate glass substrates were cleaned and P3HT-quencher solutions were prepared as before. 1 mL of solution was drop-cast onto the clean substrates on a hot plate at 60 °C in order to form a thick, opaque film that contained no solvent. For the x-ray diffraction data of PCBM and the radical small molecules, the films were prepared in the same manner as above using solutions of the material in chloroform. The data were obtained using a Rigaku SmartLab X-ray diffractometer with a Cu K α radiation source. All diffraction data were collected in air at room temperature.

Computational Methods

Charge transfer rates were modeled via semi-classical Marcus theory, using density functional theory (DFT) to calculate the various Marcus parameters for each molecular species in combination with P3HT. The charge-transfer rate is given by the following expression.³²

$$k_{ET} = \frac{2\pi}{\hbar} (H_{AB})^2 \frac{1}{\sqrt{4\pi\lambda k_B T}} \exp\left(-\frac{(\Delta G_0 + \lambda)^2}{4\lambda k_B T}\right) \quad (2)$$

Here H_{AB} is the electronic coupling between the initial and final electronic states, λ is the reorganization energy, and ΔG_0 is the Gibbs free energy for the charge transfer. To reduce the computational time, quaterthiophene (4T) was used as a model for P3HT and the *tert*-butyl groups of the galvinoxyl radical were replaced with methyl groups, referred to hereafter as GxMe. The optimized ground state geometry for all the neutral species, the 4T cation, and the anions of the radical species were computed at the dispersion-corrected³³ B3LYP³⁴/def2-TZVP³⁵ level of theory, as implemented in ORCA.³⁶ All geometries were confirmed by frequency calculations. For the calculation of the reorganization energy, additional single-point calculations were performed on each of the neutral species in the optimized charged geometries, and the charged species in the optimized neutral geometries. To determine the optimal separation of 4T with the individual radicals, a series of single-point calculations were performed on pairs of molecules to characterize the radial dependence of the ground state energy (Figure S1). While the equilibrium vacuum separations for the pairs were not all equal, a representative value of 4.5 Å was used in all of the following calculations for direct comparison. Finally, the excited-state energy for 4T was also calculated using time-dependent DFT (TDDFT) at the same level of theory.³⁷

The Coulombic interaction of the cation and anion leads to a substantial stabilization of the final charge transfer state, which was calculated by computing the Coulomb potential between the nuclei on the cation and the anion, using the CHELPG point charges on each of the nuclei as computed by

ORCA for the isolated 4T cation and various anions. The following formula was used.

$$E_{Coul} = \frac{1}{4\pi\epsilon_0} \sum_i^{4T \text{ Atoms}} \sum_j^{Quencher \text{ Atoms}} \frac{q_i q_j}{|\vec{r}_i - \vec{r}_j|} \quad (3)$$

Here ϵ_0 is the permittivity of free space, q_i and q_j are the CHELPG charges on the 4T cation and quencher anion nuclei, r_i and r_j are the position vectors of the 4T cation and quencher anion nuclei, and i and j are summed over the 4T cation and quencher anion atoms, respectively. From these calculations, the Gibbs free energy change was calculated using the following formula.

$$\Delta G_0 = (E_{4T^+,CG} + E_{Q^-,CG} + E_{Coul}) - (E_{4T,NG} + E_{Q,NG} + \Delta E_{Ex,4T}) \quad (4)$$

Here, the subscripts CG and NG refer to the single point energy of the optimized geometries of the charged and neutral species, respectively; $\Delta E_{Ex,4T}$ refers to the energy difference between the first singlet excited state and the ground state of 4T; and ΔE_{Coul} refers to the potential energy from the coulombic attraction between the two charged molecules. The reorganization energy was calculated from the following equations.

$$\lambda = \lambda_{inner} + \lambda_{outer}$$

$$\lambda_{inner} = \frac{1}{2} \{ [(E_{4T,CG} + E_{Q,CG}) - (E_{4T,NG} + E_{Q,NG})] + [(E_{4T^+,NG} + E_{Q^-,NG}) - (E_{4T,CG} + E_{Q,CG})] \}$$

$$\lambda_{outer} = \frac{1}{4\pi\epsilon_0} \left(\frac{1}{2r_{4T}} + \frac{1}{2r_Q} - \frac{1}{R} \right) \left(\frac{1}{n^2} - \frac{1}{\epsilon} \right)$$

Here ϵ is the static dielectric permittivity of the material, r_{4T} and r_Q are the radii of the 4T and quencher species, R is the distance between the 4T and quencher molecules, and n is the refractive index of the bulk material. For the inner reorganization energy (i.e., the energy difference due to the change in molecular geometry between products and reactants), Marcus theory assumes that the energy difference between the neutral molecules in the charged geometry and in the neutral geometry is the same as the energy difference between the charged molecules in the neutral geometry and in the charged geometry. In practice, these will not exactly be equal. Therefore, both differences were calculated and the average was taken. For the outer reorganization energy (i.e., the energy difference due to the relaxation of the surrounding media), the radii of the 4T and quencher species were calculated by measuring the volume of each species using the Chimera software package.^{38,39} The radius of a sphere with the equivalent volume as that of the chemical species was used as its radius. As before, 4.5 Å was used as the 4T-quencher distance. For the dielectric permittivity and refractive index, the values for P3HT, which are 3 and 1.4 respectively,^{40,41} were used.

Finally, the electronic coupling was calculated as the off-diagonal Fock matrix elements corresponding to the 4T LUMO ($\phi_{4T,LUMO}$) and radical SOMO orbitals ($\phi_{Q,SOMO}$) of the isolated molecules, with the Kohn-Sham Fock matrix of the dimer at the neutral equilibrium separation distance ($F_{4T,Q}$):

$$H_{AB} = \langle \phi_{4T,LUMO} | F_{4T,Q} | \phi_{Q,SOMO} \rangle \quad (8)$$

The rate at which FRET occurs is given by the following expression.^{18,42}

$$k_{FRET} = \frac{Q_D \kappa^2 (9000 \ln 10)}{\tau_D R^6 (128 \pi^5 N n^4)} J = \frac{1}{\tau_D} \left(\frac{R_0}{R} \right)^6 \quad (9)$$

$$J = \frac{\int_0^\infty F_D(\lambda) \varepsilon_Q(\lambda) \lambda^4 d\lambda}{\int_0^\infty F_D(\lambda) d\lambda} \quad (10)$$

Here Q_D is the quantum efficiency of the donor (0.01 for P3HT as a thin film⁴³); κ is the dipole orientation factor, which is assumed to be 2/3 for randomly oriented dipoles; τ_D is the excited state lifetime of the donor (400 ps for P3HT as a thin film⁴³); R is the donor-quencher distance; N is Avogadro's constant; n is the refractive index of the medium, and J is the overlap integral. The equation can be simplified by collapsing many of the parameters of the system into a single parameter R_0 , which corresponds to the distance at which the FRET rate is equal to the natural decay rate of the excited state. In (10), λ is the photon wavelength, $F_D(\lambda)$ is the relative fluorescence intensity of the donor species at the wavelength (normalized so that $\int_0^\infty F_D(\lambda) d\lambda = 1$), and $\varepsilon_Q(\lambda)$ is the molar absorptivity of the quencher species at the given wavelength.

Results and Discussion

Fluorescence quenching activity was observed to a variable degree for some, but not all, of the interacting radical-polymer blends evaluated. Figure 1 shows a Stern-Volmer plot of the fluorescence intensity of solutions of P3HT and the various radical quencher species versus the concentration of the quencher. For comparison, a solution mixture of P3HT and PCBM is included, as PCBM acts as an efficient fluorescence quencher for a wide variety of conjugated polymers,⁴⁴ including polythiophenes.^{45,46} All solution intensities were corrected for the inner filter effect (see the ESI for details) due to the significant absorption of the quencher species, as shown in Figure S2. Note that the full fluorescence spectra of the different mixtures are shown in Figure S3. The quenching behavior for the galvinoxyl radical is on par with that demonstrated by PCBM, suggesting that the galvinoxyl radical is an effective fluorescence quencher for P3HT. PTIO also shows significant quenching behavior, while TEMPO shows insignificant quenching behavior at the concentrations probed. In particular, PCBM shows a Stern-Volmer constant of 0.56 mM^{-1} , the galvinoxyl radical shows one of 0.46 mM^{-1} , the PTIO radical shows one of 0.29 mM^{-1} , and the TEMPO radical shows one of 0.06 mM^{-1} (Figure 1). It is worth noting that, for diffusion

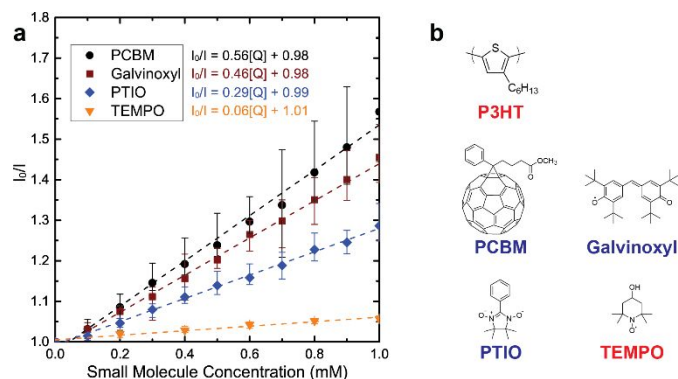


Figure 1. (a) Stern-Volmer plots of the corrected fluorescence intensity of P3HT solutions in chloroform (60 μM of thiophene repeat units) and small molecules that serve as quenching sites for the photoexcited P3HT. The vertical axis represents the intensity of a P3HT-only solution divided by the corrected intensity of a solution consisting of P3HT and the quencher at a specific concentration. These data demonstrate that the galvinoxyl and PTIO radical species have nearly the same quenching ability for P3HT as PCBM does in solution; conversely, TEMPO does not demonstrate this property. Error bars show the range of values measured for each concentration of quencher. The excitation and emission wavelengths for all of the measurements were 500 nm and 578 nm, respectively. The raw data were corrected for the inner filter effect. (b) Molecular structures of species used in this work. Electron-donating (p-type) species are indicated in red, while electron-accepting (n-type) species are indicated with blue labels.

limited quenching, direct comparisons of the Stern-Volmer constants can only be made for molecules of similar sizes. However, theory predicts that larger molecules will react slower in a diffusion-limited regime, due to the increased drag force acting on the molecule.^{47,48} Therefore, the relative trend observed in the quenching behavior would be magnified if molecular size were taken into account.

A similar trend in relative quenching behavior is seen for thin film composites of P3HT blended with the quencher species (Figure 2). This suggests that a similar mechanism is responsible for the quenching behavior in both solution and in thin films, allowing the nature of the quenching interaction to be examined from both experimental platforms. In the interest of translating these results to future device applications, we primarily utilized samples in the thin film state to probe these mechanisms. Absorbance data were used to ascertain the

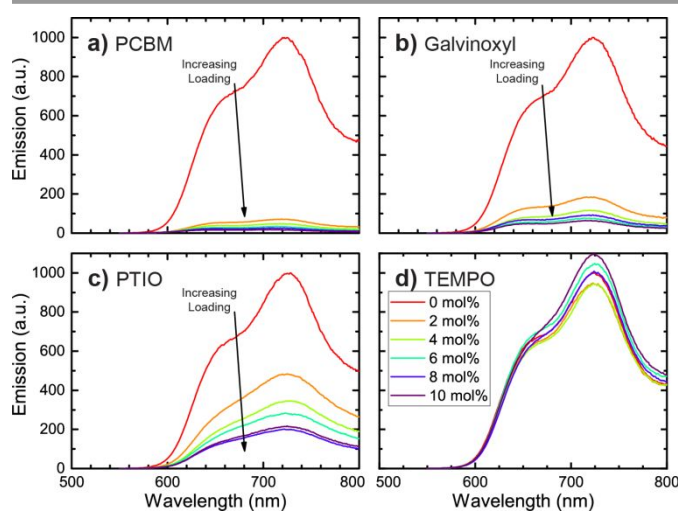


Figure 2. Reduction in intensity of fluorescence spectra of P3HT thin films with increasing loadings of (a) PCBM, (b) the galvinoxyl radical, (c) the PTIO radical, and (d) the TEMPO radical. As with the solution-state measurements, the PTIO and galvinoxyl radicals show a reduction in the P3HT fluorescence intensity in the solid state while the TEMPO radical does not. The excitation wavelength was 500 nm.

underlying nature of the quenching interaction in these soft materials systems. As can be seen from Figure , and the inset of Figure 3c, there is no apparent shift in the absorbance peaks and an absence of the appearance of any new peaks. This is seen in solution phase as well (Figure S2), and in those measurements, the total absorbance follows the Beer-Lambert law for the absorbance of the quencher species in a P3HT solution. That is, the final curve is the sum of the two independent absorption spectra, whose magnitude at all points is proportional to the concentration of species present. This suggests that the quenching observed is a dynamic quenching mechanism and not due to the formation of a non-fluorescent supramolecular complex. A blue shift in the peak near 500 nm for P3HT is visible upon the addition of PCBM, as seen in Figure 3a, which suggests that PCBM is disrupting the crystalline packing of the P3HT in the solid state, which is consistent with previous reports.⁴⁹

Interestingly, this peak shift is not observed in any of the P3HT-radical blends. This is consistent with x-ray diffraction (XRD) measurements, which show that P3HT forms pristine crystalline domains on the nanoscale (Figure). For the P3HT-radical blends, the (100) and (010) peaks remain in the same location, suggesting that the P3HT crystalline structure is unaffected by the presence of the radical species. A P3HT-PCBM blend, by contrast, shows a suppression of the (010) peak for P3HT with no appearance of the PCBM crystal peaks (Figure a), which also suggests that PCBM disrupts the crystalline packing of the P3HT, but does not form its own phase at these low loadings of the quenching species. For the P3HT-Galvinoxyl and P3HT-TEMPO blends, the primary peak corresponding to the radical species is seen in the blended films, suggesting formation of pure crystalline phases for the radical species

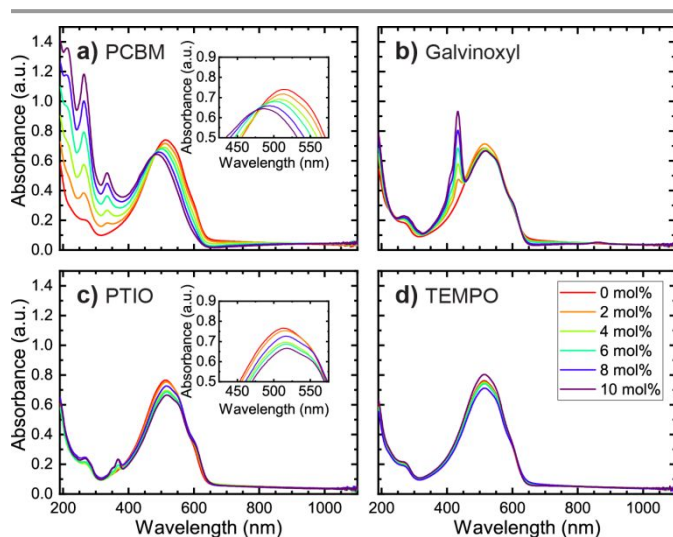


Figure 3. Absorbance spectra of P3HT thin films with increasing amounts of (a) PCBM, (b) the galvinoxyl radical, (c) the PTIO radical, and (d) the TEMPO radical. These data demonstrate that no supramolecular complexes are forming in the ground state between P3HT and the radical species, as the peak locations for P3HT and the radical species are unchanged [see inset of (c)]. Moreover, there is no appearance of a lower energy absorption band. PCBM, by contrast, shows a blue-shifting in the P3HT absorption peak [see inset of (a)], most likely because the PCBM disrupts the crystalline packing of the P3HT. The insets show the blue-shift for P3HT-PCBM in greater detail, as compared to P3HT-PTIO, which shows no shift.

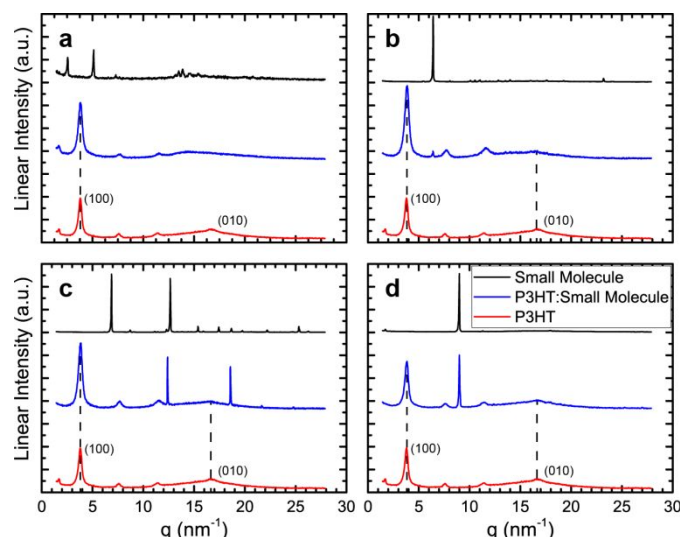


Figure 4. XRD data of P3HT thin films with small molecule additives of (a) PCBM, (b) the galvinoxyl radical, (c) the PTIO radical, and (d) the TEMPO radical present at a loading of 10% (on a molar basis), compared to those of pristine P3HT and the pristine small molecule species. For the radical species, peaks corresponding to those seen for pristine P3HT appear in the XRD spectra of the combined films (blue) with minimal shift in peak locations, indicating the existence of a pure P3HT phase in the film. This is in contrast with the P3HT-PCBM film, which shows no (010) peak corresponding to the π - π stacking, most likely because the PCBM disrupts the crystalline packing of the P3HT. The spectra are shifted vertically and the small molecule signals are scaled in order to provide clarity in data presentation.

(Figure b and d). Interestingly, two new peaks are seen for the P3HT-PTIO blend, which do not correspond to any peaks seen in either pure compound (Figure c). As the peaks corresponding to the pristine PTIO radical are not seen, this suggests that the crystal structure of the PTIO radical is disrupted. However, as a pristine P3HT phase is present in the blended film, it is still reasonable to conclude that the quenching behavior seen in P3HT-PTIO blends is not due to a change in the crystal structure of the fluorescent species.

These trends in quenching data and nanoscale structure are consistent with one of two interaction mechanisms: either (1) photoinduced charge transfer or (2) excited state transfer through a Förster Resonance Energy Transfer (FRET) or Dexter Energy Transfer pathway.¹⁸ The excited state transfer mechanisms are similar in that they both result in the fluorescent molecule, or donor, being returned to the ground electronic state, while the quencher, or acceptor, is promoted to an excited state. Both require an electronic transition for both the donor and acceptor with the same energy change. However, they differ in the mechanism by which they occur. FRET occurs via a resonant interaction between the excitation dipoles,⁴² while Dexter transfer happens due to a concerted electron and hole transfer from the donor to the acceptor.⁵⁰ Two functional differences exist between the two mechanisms. First, as FRET is mediated by dipole interactions its rate is inversely proportional to the distance to the sixth power, while Dexter transfer, which relies on overlap between the frontier molecular orbitals of the donor and acceptor species, shows approximately an exponential dependence on distance. Therefore, FRET is able to operate at large distances, while Dexter transfer is limited to molecules in close proximity.

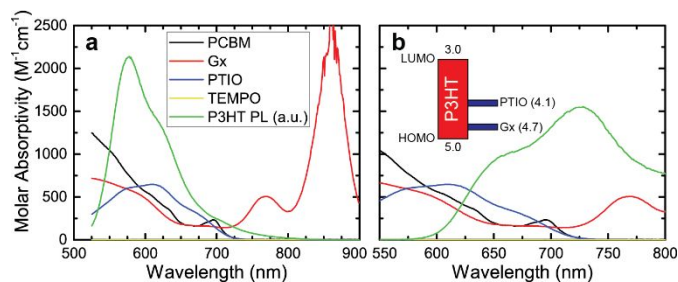


Figure 5. Overlap of the P3HT emission spectrum (green line) with the absorbance spectra of the quencher molecules. (a) The emission spectrum of a 60 μM P3HT solution in chloroform, and (b) the emission spectrum of a P3HT thin film. The inset shows the frontier orbital (HOMO and LUMO) energies of P3HT and the reduction potentials, in units of eV removed from free vacuum, of the two n-type open-shell species: the PTIO and galvinoxyl radicals.

Second, for FRET to occur both excited state transitions require a transition dipole, while Dexter transfer can occur as long as two isoenergetic electronic transitions exist, allowing for the acceptor to be promoted to a non-optically active excited state or one with a different spin state. Because of these two factors, typically if there is an overlap of the fluorescence spectrum of the donor with the absorbance spectrum of the acceptor, FRET is considered to be the dominant mechanism, with Dexter transfer being considered only when FRET is not possible.

Both the galvinoxyl and PTIO radicals show significant absorbance coefficients within the region of the spectrum where P3HT emits, both in solution phase and in solid state (**Error! Reference source not found.**), due to their extensive π -conjugation. TEMPO, by contrast, shows minimal absorbance in that region. This spectral overlap suggests that FRET may be the mechanism for the observed quenching. Because of the discussion above and because these transitions are dipole-allowed, we will not consider Dexter further, though its contribution could be measured by using covalently-linked P3HT-radical hybrid materials and tracking the distance dependence of the quenching. However, the observed trend in quenching behavior is also consistent with photoinduced electron transfer as a mechanism. In thin films, the fluorescence quenching of P3HT by PCBM is caused by such a mechanism,⁵¹ and based upon the observed redox behavior of the radical species, a photoinduced electron transfer mechanism is energetically viable.

The galvinoxyl and PTIO radicals show a reduction potential of 4.7 and 4.1 eV below vacuum, respectively.^{52,53} These values are farther-removed from vacuum than that of the lowest unoccupied molecular orbital (LUMO) energy of P3HT, which is 3.0 eV below vacuum, indicating that an electron transfer from an excited P3HT to one of these radical species could occur (inset of **Error! Reference source not found.**). The TEMPO radical, by contrast, has never been observed to form a stable anion species, suggesting that it would be unable to act as an electron acceptor. The presence of π -conjugation may also play a role in the stability of the anion species, though introduction of electron-withdrawing groups has also been utilized to design n-type radical species.⁵⁴ Nevertheless, as both mechanisms are consistent with the observed trend, and have similar origins from a molecular structure standpoint, further

characterizations are necessary to quantify the relative importance of the different mechanisms.

To uncover which mechanisms are at play in these optoelectronically-active blends, transient absorption spectra of the P3HT-radical blends were compared with the spectrum of pristine P3HT (Figure). The spectrum of pristine P3HT shows a bleach signal between 500 and 600 nm, corresponding to the ground-state bleach (GSB), as well as a photoinduced absorption between 600 and 700 nm, corresponding to photoinduced absorption of delocalized polarons (i.e., positively-charged P3HT segments within crystalline regions of the thin film).⁵⁵ Comparing this spectrum with the spectra associated with those of the P3HT-radical blends shows little qualitative difference. That is, no additional signals corresponding to bleaching of the radicals or photoinduced absorption of their anions can be detected. In the case of the galvinoxyl radical, the main absorbance peak is found at 400 nm, outside the range of the detector. The galvinoxyl anion, however, absorbs strongly at 560 nm, well within the range measured (Figure S4). No clear difference can be seen between the spectra at this point, suggesting that photoinduced charge transfer is not at play, despite the energetic favorability of such a transfer. In the case of PTIO, the main absorbance peak overlaps with that of P3HT, and the anion absorbs around 325 nm, also outside the range that can be measured by the available equipment. Nevertheless, a clear difference is seen between the P3HT-radical blends and the P3HT-PCBM blend,

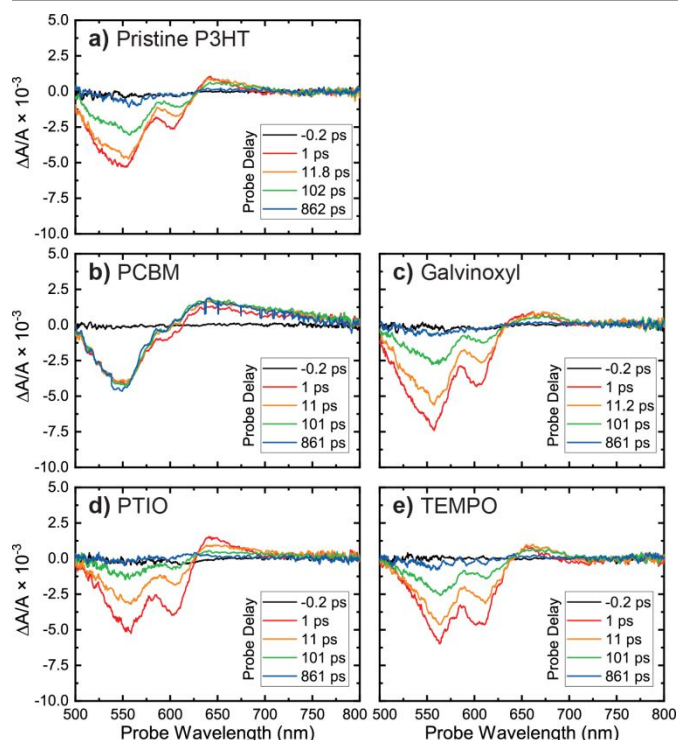


Figure 6. Representative transient absorption spectra of a (a) pristine P3HT film, (b) P3HT-PCBM blend, (c) P3HT-Galvinoxyl blend, (d) P3HT-PTIO blend, and (e) P3HT-TEMPO blend at selected delay times. The negative signal from 500 to 625 nm corresponds to the ground-state bleaching of the P3HT film, while the positive signal from 625 to 700 nm corresponds to delocalized polarons in the P3HT film. The pump wavelength was 400 nm. All quencher species were added to the thin films at a 10 mol% loading.

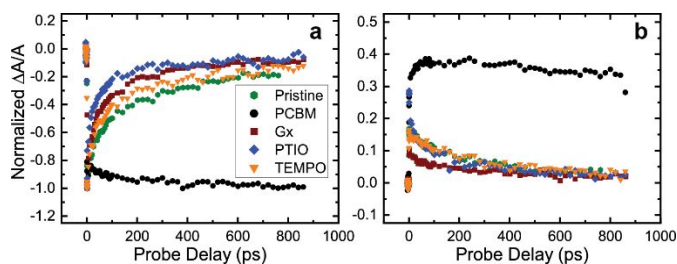


Figure 7. Comparison of the dynamics of the transient absorption signals of the P3HT-quencher blends at a probe wavelength of (a) 550 nm (ground-state bleach) and (b) 650 nm (polaron). Each of the radical-containing composites shows a faster decay of both signals over the pristine sample. This is in contrast to the P3HT-PCBM blend, which shows a persistent signal over the course of the measurement that reaches a maximum long after the P3HT-radical blends, due to persistent charge separation. A 10 mol% loading of quencher species was used for the films.

which does show charge transfer. A larger polaron signal is present, and the signal persists for the entire measurement, which is consistent with photoinduced charge separation.^{51,56,57} The lack of similar signals suggests that charge transfer is not occurring in the P3HT-radical blends.

The data in the time domain reveal a clear difference in behavior between the pristine P3HT and the P3HT-radical composite films (**Error! Reference source not found.**). For the P3HT-radical blends, both the GSB and the polaron signals decay significantly more rapidly than for the pristine film, suggesting that the radicals enhance the rate of ground state recovery. This is in stark contrast to the P3HT-PCBM film, where the ground state bleach and polaron signals persist with minimal decay through the duration of the experiment, due to the long-term charge separation. Additionally, the dynamics of the GSB and polaron signals appear to track each other well for both the pristine and radical-doped films, which suggests that the presence of the radicals has little effect on the formation of polarons within the film.

This clear contrast between P3HT-PCBM and the radical signals, as well as the absence of any signals corresponding to the anions of the radical acceptors within the wavelength window probed, suggests that charge transfer is minimal in these blends. However, the increased rate of decay for the GSB is consistent with FRET as a mechanism, as resonant energy transfer results in regeneration of the ground state of the donor. Therefore, FRET appears to be the dominant mechanism behind the observed fluorescence quenching.

To further assist with the determination of the quenching mechanism, computational studies were performed on P3HT in combination with the different quencher species to estimate the rate of the charge transfer reaction and compare this to the FRET rate (see methods section for further details and a description of all the parameters). To reduce the computational time, quaterthiophene (4T) was used as a substitute for P3HT, and the *tert*-butyl moieties on the galvinoxyl radical were replaced with methyl groups, referred hereafter as GxMe. To facilitate a direct comparison, after being oriented in a cofacial manner as described in the ESI, the centroid-centroid distance was set at 4.5 Å. While the equilibrium separation for the 4T-GxMe pair was significantly smaller at 3.9 Å (Figure S1), the reduced steric hindrance of the GxMe molecule compared to Gx means that a larger separation would be expected for a 4T-Gx

pairing. This distance is also larger than what is typically seen for studies on photoinduced charge transfer in P3HT-PCBM,^{40,58} again, this is due to the increased steric hindrance from the radical species. The results of the calculations for the charge transfer rates are shown in **Error! Reference source not found.**

As predicted from the orbital energies and the reduction potentials, electron transfer from 4T to GxMe is calculated to be favorable and electron transfer from 4T to TEMPO is unfavorable. Interestingly, electron transfer to PTIO is calculated to be unfavorable, contrary to the predictions from its measured reduction potential. However, this energy is lower than the reorganizational energy. Ultimately, this combined with the large electronic coupling leads to a significant charge transfer rate of $3.7 \times 10^8 \text{ s}^{-1}$. For GxMe, while the electron transfer is energetically favorable, the reaction is significantly within the Marcus inverted region, which results in a negligible charge transfer rate. In the case of TEMPO, the electron transfer is unfavorable and thus the charge transfer rate is also negligible. The insignificant charge transfer rate predicted for the 4T-GxMe pair is inconsistent with charge transfer being the primary mechanism behind the fluorescence quenching interaction.

By utilizing the spectral data and assuming an intermolecular separation of 4.5 Å, the FRET rates can be computed. The calculated values are shown in **Error! Reference source not found.** As predicted from the spectral overlap, both the galvinoxyl and PTIO radicals show a significant quenching rate through the FRET mechanism. TEMPO, by contrast, gives a rate 4 orders of magnitude slower. Thus, the calculated FRET rates agree with the trend observed in quenching behavior. Additionally, for the PTIO radical, the calculated FRET rate is 3 orders of magnitude faster than the calculated charge transfer rate, which agrees with the lack of observed charge transfer in the experimental results. Therefore, these computational results are consistent with the experimental results and indicate that FRET is the dominant quenching mechanism in the P3HT-radical blends.

Table 1. Calculated Charge Transfer Parameters and Rates for the Radical Species.

Quencher	ΔG_0 (eV)	H_{AB} (meV)	λ_{inner} (eV)	λ_{outer} (eV)	k_{ET} (s^{-1})
GxMe	-1.53	-9.2	0.21	0.10	3.8×10^{-8}
PTIO	0.27	-95.6	0.61	0.11	3.7×10^8
TEMPO	0.99	23.2	0.81	0.14	1.9×10^{-4}

Table 2. Calculated FRET Parameters and Rates for P3HT-Radical Blends.

Quencher	J ($\text{nm}^4 \text{ M}^{-1} \text{ cm}^{-1}$)	R_0 (Å)	k_{FRET} (s^{-1})
Galvinoxyl	7.19×10^{13}	13.9	2.2×10^{12}
PTIO	2.95×10^{13}	12.0	9.0×10^{11}
TEMPO	2.34×10^{10}	3.7	7.7×10^8

Conclusions

The electronic and energetic interactions between open-shell small molecules and a common conjugated polymer, P3HT,

in solution and as composite thin films were evaluated in full. Specifically, the fluorescence of P3HT was observed to be effectively quenched by the stable organic open-shell species, the galvinoxyl and PTIO radicals both in solution and as thin films, with quenching performance on par with that of PCBM. The TEMPO radical, by contrast, showed minimal quenching of the P3HT fluorescence. As demonstrated through a combination of computation, steady-state spectroscopy, and ultrafast spectroscopy, the quenching behavior was primarily due to energy transfer between the two species, in contrast to the electron-transfer mechanism that is dominant in the classic closed-shell quencher PCBM. This mechanism was supported by the large spectral overlap between the absorbance spectra of the radical species that acted as quenchers and the emission spectrum of the P3HT donor, as well as the rapid recovery of the ground state observed through transient absorption measurements. Charge transfer, an alternative plausible mechanism, was determined to not be the primary means of fluorescence quenching in the P3HT-radical systems evaluated here as the signal of the quencher anions were not observed in the transient absorption, as well as through calculations that suggested it would proceed at a far slower rate than through FRET. As FRET is a long-range interaction, this finding has implications for future applications involving energy transfer from a fluorescent conjugated molecule to an open shell species, such as heterojunctions between the two in device applications or in conjugated molecules bearing radical pendant groups. Specifically, the finding suggests that by choosing a radical species that can act as a FRET acceptor for a given conjugated species, greater flexibility in the distance between the two moieties can be achieved. Moreover, it highlights the key need to appropriately and fully evaluate the subtle physical, electronic, and energetic interactions between closed-shell and open-shell organic composite materials.

Conflicts of interest

There are no conflicts to declare.

Acknowledgements

The work performed by D.A.W. and B.W.B. was made possible through the Air Force Office of Scientific Research (AFOSR) under support provided by the Organic Materials Chemistry Program (Grant Number: FA9550-15-1-0449, Program Manager: Dr. Kenneth Caster), and we gratefully thank the AFOSR for this support. J.M.S and L.H. acknowledge the support from US National Science Foundation through grant NSF-CHE-1555005 for the transient absorption characterization.

Notes and references

- 1 G. Meller and T. Grasser, *Organic Electronics*, Springer, Heidelberg/New York, 2010.
- 2 R. Ma, in *Handbook of Visual Display Technology*, eds. J.

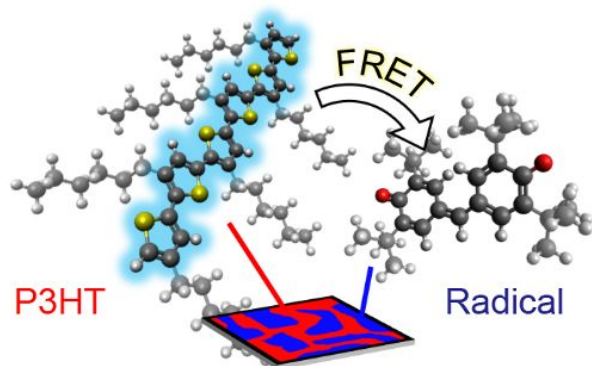
- 3 Chen, W. Cranton and M. Fihn, Springer, 2nd edn., 2016, pp. 1799–1820.
- 4 B. W. Boudouris, *Curr. Opin. Chem. Eng.*, 2013, **2**, 294–301.
- 5 A. Facchetti, *Chem. Mater.*, 2011, **23**, 733–758.
- 6 S. Mukherjee and B. W. Boudouris, *Organic Radical Polymers: New Avenues in Organic Electronics*, Springer, 2017.
- 7 D. A. Wilcox, V. Agarkar, S. Mukherjee and B. W. Boudouris, *Annu. Rev. Chem. Biomol. Eng.*, 2018, **9**, 83–103.
- 8 Y. Joo, V. Agarkar, S. H. Sung, B. M. Savoie and B. W. Boudouris, *Science*, 2018, **359**, 1391–1395.
- 9 L. Rostro, L. Galicia and B. W. Boudouris, *J. Polym. Sci. B Polym. Phys.*, 2015, **53**, 311–316.
- 10 L. Zheng, S. Mukherjee, K. Wang, M. E. Hay, B. W. Boudouris and X. Gong, *J. Mater. Chem. A*, 2017, **5**, 23831–23839.
- 11 S. H. Sung, N. Bajaj, J. F. Rhoads, G. T. Chiu and B. W. Boudouris, *Org. Electron.*, 2016, **37**, 148–154.
- 12 E. P. Tomlinson, M. J. Willmore, X. Zhu, S. W. A. Hilsmier and B. W. Boudouris, *ACS Appl. Mater. Interfaces*, 2015, **7**, 18195–18200.
- 13 E. P. Tomlinson, S. Mukherjee and B. W. Boudouris, *Org. Electron.*, 2017, **51**, 243–248.
- 14 Y. Joo, L. Huang, N. Eedugurala, A. E. London, A. Kumar, B. M. Wong, B. W. Boudouris and J. D. Azoulay, *Macromolecules*, 2018, **51**, 3886–3894.
- 15 T. P. Basel, U. Huynh, T. Zheng, T. Xu, L. Yu and Z. V. Vardeny, *Adv. Funct. Mater.*, 2015, **25**, 1895–1902.
- 16 F. Li, D. N. Gore, S. Wang and J. L. Lutkenhaus, *Angew. Chem. Int. Ed.*, 2017, **56**, 9856–9859.
- 17 Y. Zhang, A. M. Park, S. R. McMillan, N. J. Harmon, M. E. Flatté, G. D. Fuchs and C. K. Ober, *Chem. Mater.*, 2018, **30**, 4799–4807.
- 18 F. Li, S. Wang, Y. Zhang and J. L. Lutkenhaus, *Chem. Mater.*, 2018, **30**, 5169–5174.
- 19 J. R. Lakowicz, *Principles of Fluorescence Spectroscopy*, Springer, New York, 3rd edn., 2010.
- 20 Q. Peng, A. Obolda, M. Zhang and F. Li, *Angew. Chem. Int. Ed.*, 2015, **54**, 7091–7095.
- 21 E. Neier, R. Arias, N. Rady, S. Venkatesan, T. W. Hudnall and A. Zakhidov, *Org. Electron.*, 2017, **44**, 126–131.
- 22 S. A. Green, D. J. Simpson, G. Zhou, P. S. Ho and N. V. Blough, *J. Am. Chem. Soc.*, 1990, **112**, 7337–7346.
- 23 Y. Kawanaka, A. Shimizu, T. Shinada, R. Tanaka and Y. Teki, *Angew. Chem. Int. Ed.*, 2013, **52**, 6643–6647.
- 24 B. K. Hughes, W. A. Braunecker, A. J. Ferguson, T. W. Kemper, R. E. Larsen and T. Gennett, *J. Phys. Chem. B*, 2014, **118**, 12541–12548.
- 25 K. Zamojć, W. Wiczak, B. Zaborowski, D. Jacewicz and L. Chmurzyński, *Spectrochim. Acta - Part A Mol. Biomol. Spectrosc.*, 2015, **136**, 1875–1880.
- 26 H. Gustmann, D. Lefrancois, A. J. Reuss, D. B. Gophane, M. Braun, A. Dreuw, S. T. Sigurdsson and J. Wachtveitl, *Phys. Chem. Chem. Phys.*, 2017, **19**, 26255–26264.
- 27 C. Tansakul, E. Lilie, E. D. Walter, I. Rivera, Frank, A. Wolcott, J. Z. Zhang, G. L. Millhauser and R. Braslau, *J. Phys.*

- Chem. C*, 2010, **114**, 7793–7805.
- 27 F. Lin, D. Pei, W. He, Z. Huang, Y. Huang and X. Guo, *J. Mater. Chem.*, 2012, **22**, 11801.
- 28 P. Dutta and R. Beaulac, *Chem. Mater.*, 2016, **28**, 1076–1084.
- 29 A. Marrocchi, D. Lanari, A. Facchetti and L. Vaccaro, *Energy Environ. Sci.*, 2012, **5**, 8457.
- 30 A. V. Fonin, A. I. Sulatskaya, I. M. Kuznetsova and K. K. Turoverov, *PLoS One*, 2014, **9**, e103878.
- 31 C. A. Parker and W. J. Barnes, *Analyst*, 1957, **82**, 606–618.
- 32 R. Marcus and N. Sutin, *Biochim. Biophys. Acta-Reviews Bioenerg.*, 1985, **811**, 265–322.
- 33 S. Grimme, S. Ehrlich and L. Goerigk, *J. Comput. Chem.*, 2009, **32**, 1456–1465.
- 34 A. D. Becke, *J. Chem. Phys.*, 1993, **98**, 5648.
- 35 F. Weigend and R. Ahlrichs, *Phys. Chem. Chem. Phys.*, 2005, **7**, 3297.
- 36 F. Neese, *Wiley Interdiscip. Rev. Comput. Mol. Sci.*, 2012, **2**, 73–78.
- 37 T. Petrenko, S. Kossmann and F. Neese, *J. Chem. Phys.*, 2011, **134**, 0–14.
- 38 E. F. Pettersen, T. D. Goddard, C. C. Huang, G. S. Couch, D. M. Greenblatt, E. C. Meng and T. E. Ferrin, *J. Comput. Chem.*, 2004, **25**, 1605–1612.
- 39 M. F. Sanner, A. J. Olson and J.-C. Spohner, *Biopolymers*, 1996, **38**, 305–320.
- 40 T. Liu and A. Troisi, *J. Phys. Chem. C*, 2011, **115**, 2406–2415.
- 41 A. Hamnett and A. R. Hillman, *J. Electrochem. Soc.*, 1988, **135**, 2517–2524.
- 42 T. Förster, *Radiat. Res. Suppl.*, 1960, **2**, 326–339.
- 43 S. Cook, A. Furube and R. Katoh, *Energy Environ. Sci.*, 2008, **1**, 294.
- 44 J. Wang, D. Wang, D. Moses and A. J. Heeger, *J. Appl. Polym. Sci.*, 2001, **82**, 2553–2557.
- 45 T. Yamashiro, Y. Aso, T. Otsubo, H. Tang, Y. Harima and K. Yamashita, *Chem. Lett.*, 1999, **28**, 443–444.
- 46 B. W. Boudouris, F. Molins, D. A. Blank, C. D. Frisbie and M. A. Hillmyer, *Macromolecules*, 2009, **42**, 4118–4126.
- 47 J. Q. Umberger and V. K. LaMer, *J. Am. Chem. Soc.*, 1945, **67**, 1099–1109.
- 48 R. A. Alberty and G. G. Hammes, *J. Phys. Chem.*, 1958, **62**, 154–159.
- 49 P. Vanlaeke, A. Swinnen, I. Haeldermans, G. Vanhoyland, T. Aernouts, D. Cheyns, C. Deibel, J. D’Haen, P. Heremans, J. Poortmans and J. V. Manca, *Sol. Energy Mater. Sol. Cells*, 2006, **90**, 2150–2158.
- 50 D. L. Dexter, *J. Chem. Phys.*, 1953, **21**, 836–850.
- 51 I. W. Hwang, D. Moses and A. J. Heeger, *J. Phys. Chem. C*, 2008, **112**, 4350–4354.
- 52 T. Suga, H. Ohshiro, S. Ugita, K. Oyaizu and H. Nishide, *Adv. Mater.*, 2009, **21**, 1627–1630.
- 53 T. Suga, S. Sugita, H. Ohshiro, K. Oyaizu and H. Nishide, *Adv. Mater.*, 2011, **23**, 751–754.
- 54 T. Suga, Y. J. Pu, S. Kasatori and H. Nishide, *Macromolecules*, 2007, **40**, 3167–3173.
- 55 X. M. Jiang, R. Österbacka, O. Korovyanko, C. P. An, B. Horovitz, R. A. J. Janssen and Z. V. Vardeny, *Adv. Funct. Mater.*, 2002, **12**, 587–597.
- 56 J. Piris, T. E. Dykstra, A. A. Bakulin, P. H. M. Van Loosdrecht, W. Knulst, M. T. Trinh, J. M. Schins and L. D. A. Siebbeles, *J. Phys. Chem. C*, 2009, **113**, 14500–14506.
- 57 J. Guo, H. Ohkita, H. Benten and S. Ito, *J. Am. Chem. Soc.*, 2010, **132**, 6154–6164.
- 58 Y. Kanai and J. C. Grossman, *Nano Lett.*, 2007, **7**, 1967–1972.

For Table of Contents Purposes Only

Title: Tuning the Interfacial and Energetic Interactions between a Photoexcited Conjugated Polymer and Open-Shell Small Molecules

Authors: Daniel A. Wilcox, Jordan Snaider, Sanjoy Mukherjee, Long Yuan, Libai Huang, Brett M. Savoie, and Bryan W. Boudouris

TOC Image:

TOC Sentence: Photoexcited conjugated polymers are capable of exchanging energy with open-shell small molecules through a Förster Resonance Energy Transfer (FRET) mechanism.